T cell receptor binding kinetics required for T cell activation depend on the density of cognate ligand on the antigen-presenting cell

Pablo A. González*, Leandro J. Carreño*, Daniel Coombs†, Jorge E. Mora*, Edith Palmieri‡, Byron Goldstein§, Stanley G. Nathenson‡, and Alexis M. Kalergis*‡¶

*Departamento de Genética Molecular y Microbiología, Facultad de Ciencias Biológicas, Pontificia Universidad Católica de Chile, Santiago 8331010, Chile; †Department of Mathematics, University of British Columbia, Vancouver, BC, Canada V6T 1Z2; ‡Department of Microbiology and Immunology, Albert Einstein College of Medicine, Bronx, NY 10461; and §Theoretical Biology and Biophysics Group, Theoretical Division, Los Alamos National Laboratory, MS K710, Los Alamos, NM 87545

Contributed by Stanley G. Nathenson, February 6, 2005

CD8$^+$ T cells recognize peptides of eight to nine amino acid residues long in the context of MHC class I molecules on the surface of antigen-presenting cells (APCs). This recognition event is highly sensitive, as evidenced by the fact that T cells can be activated by cognate peptide/MHC complex (pMHC) at extremely low densities (1–50 molecules). High sensitivity is particularly valuable for detection of antigens at low density, such as those derived from tumor cells and intracellular pathogens, which can down-modulate cognate pMHCs from the surface of APCs to evade recognition by the adaptive immune system. T cell activation is only triggered in response to interactions between the T cell receptor (TCR) and the pMHC ligand that reach a specific half-life threshold. However, interactions with excessively long half-lives result in impaired T cell activation. Thus, efficient T cell activation by pMHC on the surface of APCs requires an optimal dwell time of TCR–pMHC interaction. Here, we show that, although this is a requirement at low cognate pMHC density on the APC surface, at high epitope density there is no impairment of T cell activation by extended TCR–pMHC dwell times. This observation was predicted by mathematical simulations for T cell activation by pMHC at different densities and supported by experiments performed on APCs selected for varied expression of cognate pMHC. According to these results, effective T cell activation depends on a complex interplay between inherent TCR–pMHC binding kinetics and the epitope density on the APC.

Activation of CD8$^+$ T cells by antigenic peptides bound to MHC class I molecules involves the engagement of T cell receptors (TCRs) on the surface of the cytotoxic T lymphocyte (CTL) by peptide/MHC complex (pMHC) on the surface of the target cell (1–3). The observation that as few as 1–50 pMHCs are sufficient to trigger CTL activation and cause lysis of target cells indicates that antigen recognition is an extremely sensitive process (4–6). The need for the detection of low-density pMHCs is exemplified by the fact that intracellular pathogens such as viruses and bacteria have evolved molecular mechanisms to avoid T cell recognition by reducing the density of MHC molecules loaded with pathogen-derived peptides on the surface of infected cells (7–10). Similarly, malignant tumors evade T cell recognition by significantly reducing surface expression of MHC molecules loaded with antigenic peptides (11, 12). Because the sustained TCR signaling required for T cell activation must be provided by a few cognate pMHC molecules on the surface of target cells, it has been suggested that a single pMHC molecule can serially engage several independent TCR molecules (6, 13–15). This serial engagement of TCRs would allow amplification of intracellular signals required for T cell activation (6, 13, 14, 16). Consistent with this model is the observation that TCR–pMHC interactions are generally of low affinity (micromolar range) and have rapid association and dissociation kinetics (4, 17). To accomplish serial engagement of multiple TCRs by a single cognate pMHC ligand, the pMHC must bind and dissociate from each TCR with fast enough kinetics to allow the next TCR to be engaged, resulting in sustained TCR signaling (1, 16, 18–20). As initially postulated by the kinetic proofreading model (21, 22) and subsequently shown experimentally (19, 20, 23, 24), a minimal or threshold half-life for the TCR–pMHC interaction is also required for productive TCR signaling. According to this model, premature TCR dissociation from the pMHC would lead to incomplete TCR signaling, preventing T cell activation. In support of this model is the observation that, in general, T cell activation correlates with the half-life of the TCR–pMHC interaction (19, 24, 25). Thus, agonist pMHC ligands show half-lives of interaction with the TCR above a certain threshold, whereas antagonist and null ligands show half-lives below this threshold (19, 24, 25).

Fulfilling the requirements of TCR serial engagement and kinetic proofreading would involve the existence of an optimal TCR–pMHC half-life for T cell activation (6, 16, 20, 26). Empirical data supporting this notion come from several independent experimental systems, where both shortened and prolonged engagement of TCR by pMHC can be detrimental for T cell activation. Although short half-lives prevent completion of TCR signaling, longer half-lives hamper TCR serial engagement by limiting the number of pMHC molecules available (19, 20, 27–30). The biological significance of inhibition of T cell activation by an extended TCR–pMHC interaction is revealed by the lack of affinity maturation during T cell responses to a virus (31), as well as by the observation that T cell clones expressing high-affinity TCRs can be impaired for activation and function (32, 33).

In this study we have generated a mathematical model to address the implications of pMHC density and TCR–pMHC dwell time on T cell activation. Simulations performed with the model suggest that increasing cognate pMHC density on the antigen-presenting cell (APC) surface diminishes the requirement of TCR serial engagement for T cell activation. Data derived from experiments performed with APCs selected for variable expression of pMHC densities support this model by showing that inhibition of T cell activation by TCR–pMHC interactions with prolonged dwell times only occurs at low (physiological) cognate pMHC densities on the APC surface. Thus, we show that by increasing the density of cognate pMHC an optimal dwell time is no longer required and T cell activation increases as a function of the TCR–pMHC interaction half-life. These observations suggest that at high epitope density kinetic proofreading remains a requirement for T cell activation, whereas TCR serial engagement becomes less stringent as the density of epitope increases on the APC surface.

Abbreviations: pMHC, peptide/MHC complex; APC, antigen-presenting cell; TCR, T cell receptor; VSV, vesicular stomatitis virus; PMA, phorbol 12-myristate 13-acetate.

¶To whom correspondence should be addressed. E-mail: kalergis@bio.puc.cl.

www.pnas.org/cgi/doi/10.1073/pnas.0500922102

Table 1. Parameter values used for TCR internalization mathematical modeling

Description	Estimate
Initial number of TCR	30×10^3
Diffusion constants of TCR and pMHC, $cm^2 \cdot s^{-1}$	3×10^{-10}
On-rate of pMHC, $cm^2 \cdot s^{-1}$	1×10^{-10}
Kinetic proofreading steps	6
Kinetic proofreading rate, s^{-1}	0.25
Down-regulation rate for triggered, unbound TCR, s^{-1}	3×10^{-3}
Surface area of cells, cm^2	5×10^{-6}
Radius of contact region, cm	4.7×10^{-4}

Parameter values were assigned according to ref. 20.

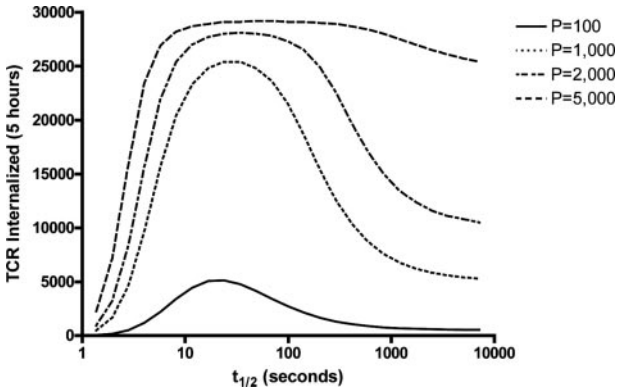

Fig. 1. Calculated levels of TCR internalization as a function of cognate pMHC density (P) and TCR–pMHC $t_{1/2}$. Results shown were generated with parameter values described in Table 1 and supposing a 5-h interaction between the T cell and the APC. TCR internalization is an increasing function of presented pMHC density on the APC surface. An optimal TCR–pMHC interaction $t_{1/2}$ for TCR internalization exists only for low pMHC densities. At higher pMHC densities this peak no longer exists and a significant increase in TCR internalization can be seen for those TCRs with prolonged TCR–pMHC interaction $t_{1/2}$.

Materials and Methods

Mathematical Model of TCR Activation and Down-Regulation. The mathematical model described in Coombs *et al.* (20) was applied here. Briefly, this model uses partial differential equations to describe the binding and unbinding of TCR and cognate pMHC along with uniform diffusion of all species in their respective membranes. The cascade of reactions after ligand binding is approximated by a kinetic proofreading system (21). TCRs completing the kinetic proofreading steps are taken to be labeled for internalization. Labeled TCRs are then internalized at one of two rates: λ_B if they are bound to pMHC and λ_T otherwise. Because TCR recycling was not considered in this model, the rate constants for TCR internalization, λ_B and λ_T, are also the rate constants for TCR degradation. Thus, the λ_B and λ_T values used here were based on published rate constants for TCR internalization (34–37). Labeled TCRs that reach the edge of the computational region (corresponding to the entire immunological synapse) revert to their original, unlabeled state. The principle readout from our model is the time course of TCR internalization. Table 1 shows the parameter values included in the model, which derive from data in ref. 20.

Cell Lines, Antibodies, and Peptides. The preparation of T cell hybridomas expressing the WT N30.7 TCR has been described (3, 19, 38). Site-directed mutagenesis of the N30.7 CDR3β leading to the V98D, V98L, G97A, G97/99A, and G99A mutants was done by cassette mutagenesis (38). The R8 cell line (H-2K$^{b/d}$) is an Abelson leukemia virus-immortalized pre-B lymphoblastoid cell line. L cells (H-2K^k) expressing H-2K^b were prepared by transfection of the H-2K^b gene as described (39). The following antibodies were used in this work: anti-TCR-β (clone H57; BD Pharmingen), anti-CD8α (clone 53-6.7; BD Pharmingen), anti-CD3ε (clone 2C11; BD Pharmingen), anti-H-2K^b (clone AF6-88.5; BD Pharmingen), anti-H-2K^b/SIINFEKL pMHC (supernatant from 25-D1.16 hybridoma provided by R. N. Germain, National Institutes of Health, Bethesda), and goat anti-mouse IgG-FITC (BD Pharmingen). The vesicular stomatitis virus (VSV) (RGYVYQGL) and ovalbumin (SIINFEKL) peptides were synthesized as described (3, 38, 40).

Activation of T Cell Hybridomas. Activation of TCR-transfected T cell hybridomas with VSV peptide-loaded APCs was done as described (38). Briefly, either 1×10^5 R8 cells (H-2K$^{b/d}$) or L-K^b cells (H-2K$^{k/b}$) pulsed with various concentrations of VSV peptide were incubated with equal numbers of T cell hybridomas, 10 ng/ml phorbol 12-myristate 13-acetate (PMA), and 20 ng/ml calcium ionophore (A23187). Activation of TCR-transfected T cell hybridomas with H-2K^b/VSV-coated plates was carried out as described (40). Briefly, 96-well plates (Corning) were coated overnight at 4°C with streptavidin (1 μg per well) and covered with different concentrations of biotinylated H-2K^b/VSV complexes. T cell hybridomas were added at 2×10^5 per well and stimulated for 24 h at 37°C. Supernatants were then harvested for IL-2 release quantification by cytokine-ELISA as described (38, 40). For antigen-independent T cell activation T cell hybridomas at 2×10^5 per well were incubated either with 50 ng per well of anti-CD3ε antibody or PMA (100 ng/ml)/A23187 (200 ng/ml).

TCR Down-Modulation Assays. A total of 2×10^5 T cell hybridomas were stimulated for 5 h either with 2×10^5 VSV-pulsed APCs (100 μM) or purified H-2K^b/VSV complexes (1 μg) adsorbed onto plastic plates. After this time, T cells were harvested and stained with anti-CD8α and anti-TCR-β antibodies for 1 h on ice, fixed with paraformaldehyde (1% in PBS), and analyzed by FACS (Becton Dickinson).

Surface Expression of H-2K^b or H-2K^b/SIINFEKL on Different APCs. Surface expression of H-2K^b on different APCs was determined by flow cytometry using the H-2K^b-specific AF6-88.5 mAb conjugated to FITC. For measuring surface density of H-2K^b/SIINFEKL complex, 5×10^5 APCs were pulsed overnight with 70 μM ovalbumin peptide and then stained with H-2K^b/SIINFEKL-specific 25-D1.16 mAb for 1 h in ice as described (8). Cells were then washed, stained with a FITC-labeled anti-mouse IgG antibody, fixed with paraformaldehyde (1% in PBS), and analyzed by FACS.

Results

Mathematical Modeling for TCR Activation. We used the mathematical model presented in Coombs *et al.* (20) to study the effect of TCR–pMHC interaction half-life and APC pMHC surface density on TCR internalization, as a parameter for T cell activation. Fig. 1 shows the predicted level of TCR down-regulation in a numerical experiment where activated TCRs are down-regulated with a larger rate after binding and dissociating from cognate pMHC (we suppose $\lambda_B = 3 \times 10^{-4} < \lambda_T = 3 \times 10^{-3}\ s^{-1}$). We observe that, for all half-life values, TCR internalization is an increasing function of presented pMHC density on the APC surface (Fig. 1). Further, we find that the previously reported peak in TCR internalization exists only at low levels of pMHC density (20). As pMHC density increases, T cells are activated more efficiently and the inhibition caused by excessively long TCR–pMHC interaction half-life is lessened (Fig. 1).

IMMUNOLOGY

Table 2. All T cell hybridomas show equivalent baseline surface expression of CD8α and TCR, as well as IL-2 release in response to CD3 or PMA-Ca^{2+} ionophore stimulation

TCR mutant	CDR3β sequence*								Surface expression†		IL-2 release‡	
	95	96	97	98	99	100	101	102	CD8α, %	TCR, %	PMA	CD3ε
WT	S	S	G	V	G	T	E	V	91.1	93.6	55.2	99.3
G97A	—	—	A	—	—	—	—	—	96.9	85.1	46.9	83.7
G97/99A	—	—	A	—	A	—	—	—	85.3	94.9	47.3	72.4
G99A	—	—	—	—	A	—	—	—	95.9	100.0	56.4	83.3
V98L	—	—	—	L	—	—	—	—	100.0	87.7	53.9	85.3
V98D	—	—	—	D	—	—	—	—	93.4	92.7	47.9	83.5

*CDR3β sequences of WT N30.7 TCR (Vβ13, Jβ1.1) and TCR mutants G97A, G97/99A, G99A, V98L, and V98D. The amino acid residue mutated is indicated.

†CD8α and TCR surface expression was determined by FACS analysis with anti-CD8α and anti-TCRβ (percentage relative to the hybridoma with the highest surface expression).

‡IL-2 release (units/ml) in response to either anti-CD3ε or PMA-Ca^{2+} ionophore stimulation.

T Cell Hybridomas Expressing TCR Mutants with Prolonged TCR–pMHC Interactions Half-Lives Are Activated Only at High pMHC Density on the APC Surface. According to the mathematical model described above, high epitope densities should be able to restore T cell activation only for those T cell hybridomas expressing mutant TCRs with prolonged $t_{1/2}$ of TCR–pMHC interaction (Table 1). To test the model we evaluated the ability of APCs with different cognate pMHC densities to activate T cell hybridomas expressing mutant TCRs shown in Table 2. pMHC density was modulated by increasing the concentration of VSV peptide and using APCs expressing different amounts of MHC-I, either R8 cells (low H-2K^b expression) or L cells transfected with the H-2K^b gene (low or high H-2K^b expression) (39).

We have previously described a set of TCR mutants derived from the H-2K^b/VSV-specific N30.7 TCR, which carry point mutations at the CDR3β loop (Table 2 and refs. 3, 19, and 38). The T cell hybridoma lines transfected either with the WT N30.7 TCR or one of the mutant TCRs display similar surface levels for TCR and CD8, as determined by flow cytometry (Table 2). Also, all T cell hybridomas secrete similar amounts of IL-2 in response to stimulation with either PMA/Ca^{2+} ionophore or TCR cross-linking by anti-CD3ε (Table 2). These results show that the TCR signaling machinery associated with the WT N30.7 TCR, as well as with all of the TCR mutants, is functional for each of the T cell hybridoma lines tested.

Although some of these TCR mutants (V98D, V98L, G99A, and G97/99A) lost the ability to be activated in response to the H-2K^b/VSV complex on the surface of R8 cells, some of them retained the ability to bind this pMHC (V98L, G99A, and G97/99A) (19). When the binding $t_{1/2}$ to H-2K^b/VSV was measured for each of these TCRs, it was observed that whereas V98L had a $t_{1/2}$ shortened by ≈10-fold, G97/99A and G99A showed a $t_{1/2}$ extended by ≈2-fold when compared with the WT N30.7 TCR (Table 3) (19).

When VSV-pulsed R8 cells were used as APCs, only T cell hybridomas expressing the WT TCR and TCR mutant G97A were activated (Fig. 2 *a* and *b* and ref. 19). Hybridomas expressing TCR mutants G97/99A, G99A, V98L, and V98D were not activated by R8 cells at any of the tested VSV concentrations (Fig. 2 *c–f* and ref. 19).

In contrast, a different pattern was observed when VSV peptide was presented on L-K^b-high cells. Because multiple copies of the H-2K^b gene were incorporated in L-K^b-high cells, these cells show an elevated H-2K^b surface expression (39). According to flow cytometry analyses, it was estimated that L-K^b-high cells express four times more surface H-2K^b than R8 cells do (Fig. 3*a*). Furthermore, when the density of a specific pMHC was determined by using mAbs specific for H-2K^b/SIINFEKL it was observed that L-K^b-high cells showed 10 times more H-2K^b/SIINFEKL complexes on their surface than R8 cells after pulsing with SIINFEKL peptide (Fig. 3*b*).

VSV-pulsed L-K^b-high cells were not only able to trigger activation of T cell hybridomas expressing the WT TCR N30.7 and TCR mutant G97A (Fig. 2 *a* and *b*), but also T cell hybridomas expressing TCR mutants G97/99A and G99A that have an extended $t_{1/2}$ of interaction with H-2K^b/VSV as compared with the WT N30.7 TCR (Fig. 2 *c* and *d* and Table 3). On the other hand, TCR mutant V98L that binds to H-2K^b/VSV with a reduced $t_{1/2}$ or TCR mutant V98D that does not bind H-2K^b/VSV were not activated by VSV-pulsed L-K^b-high cells at any of the concentrations tested (Fig. 2 *e* and *f* and Table 3). These data support the notion that high epitope densities can restore activation only for those TCR mutants with extended $t_{1/2}$ of interaction with the

Table 3. Half-life and relative efficiency of T cell activation for each T cell hybridoma pair at different epitope densities

TCR	Ligand	Half-life, *min	Relative T cell activation at low epitope density†	Relative T cell activation at high epitope density†
N30.7	K^b/VSV	5.1 ± 0.7	1	1.28 ± 0.194
G97A	K^b/VSV	5.3 ± 1.2	1.38 ± 0.012	1.35 ± 0.137
G97/99A	K^b/VSV	9.5 ± 2.1	0.16 ± 0.018	0.75 ± 0.135
G99A	K^b/VSV	10.8 ± 3.7	0.21 ± 0.039	1.23 ± 0.31
V98L	K^b/VSV	0.5 ± 0.1	0.14 ± 0.040	0.11 ± 0.011
V98D	K^b/VSV	NA	0.12 ± 0.026	0.08 ± 0.024

*TCR–ligand interaction half-lives were previously measured with H-2K^b/VSV tetramers (19). NA, not applicable because V98D does not bind H-2K^b/VSV.

†Relative T cell activation values were obtained from IL-2 release results in response to either R8 or L-K^b-high APCs pulsed with 10 μM VSV-peptide. A relative value of 1 has been given to the IL-2 release of WT N30.7 TCR bearing T cell hybridoma in response to R8 APCs pulsed with 10 μM VSV-peptide.

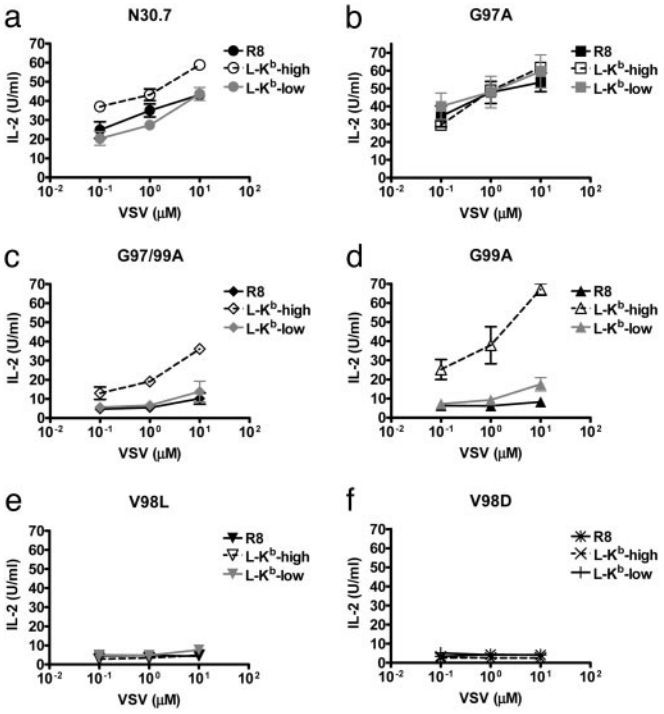

Fig. 2. T cell hybridomas expressing TCR mutants with prolonged TCR–pMHC interaction half-lives are activated only at high pMHC density on the APC surface. Data shown are units/ml IL-2 released by T cell hybridomas expressing the WT or one of the mutant TCRs in response to VSV peptide–pulsed APCs (either R8, L-K^b-low, or L-K^b-high cells). VSV-pulsed APCs were mixed with an equal number of T cell hybridomas expressing either the N30.7 TCR or one of the CDR3β mutants. After 24 h, supernatants were collected for measurement of IL-2 release. Data are means of three to five independent experiments ± SD.

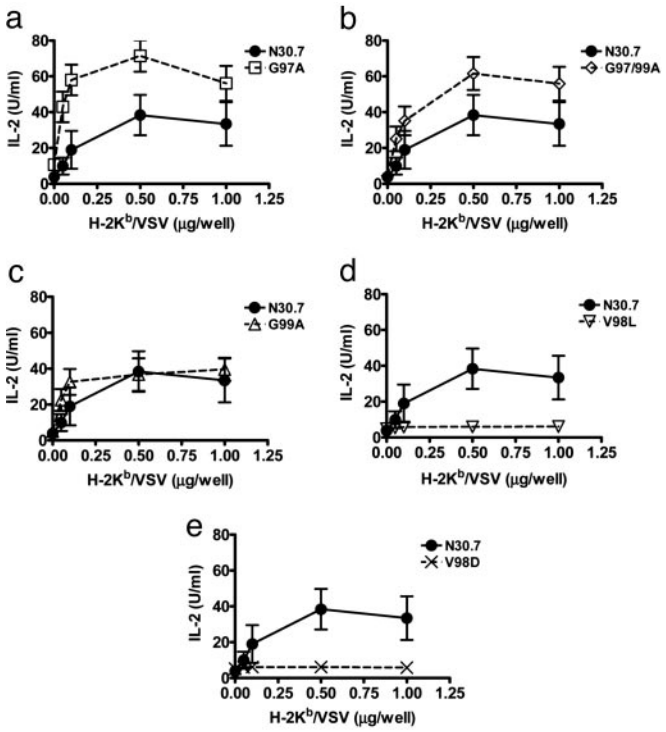

Fig. 4. Plate-bound purified pMHCs restore activation of T cell hybridomas expressing TCR mutants with prolonged TCR–pMHC interaction half-lives. IL-2 release in response to plate-bound H-2K^b/VSV complexes by T cell hybridomas expressing the WT or one of the CDR3β mutant TCRs. T cell hybridomas were cultured over increasing amounts of plate-bound H-2K^b/VSV complexes. After 24 h, supernatants were collected for measurement of IL-2 release. Data are means of four independent experiments ± SD.

pMHC ligand. To exclude the possibility that restoration of activation of T cell hybridomas with extended $t_{1/2}$ could be caused by undefined properties of L-K^b cells, we tested as APCs L-K^b cells selected for low surface expression of the H-2K^b molecule (L-K^b-low, Fig. 3). Similar to R8 cells, L-K^b-low cells expressing low-density H-2K^b were unable to activate G99A and G97/99A TCR mutants (Fig. 2). These observations indicate that L-K^b-high cells are able to restore activation of TCR mutants with extended $t_{1/2}$ only when expressing a high surface density of H-2K^b.

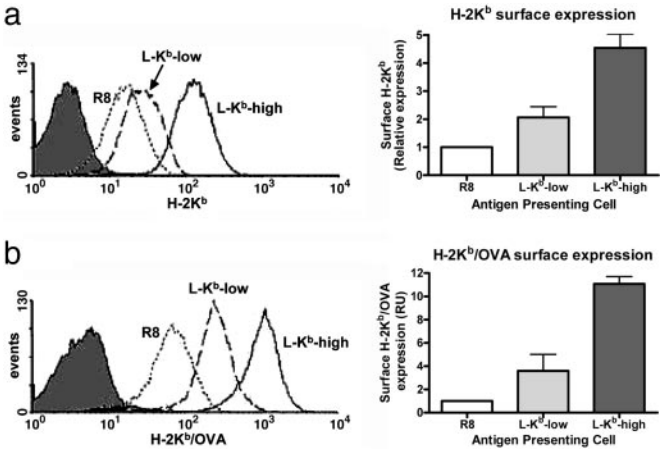

Fig. 3. L-K^b-high cells express higher surface levels of pMHCs as compared with R8 cells. Surface H-2K^b and H-2K^b/SIINFEKL complex expression was determined by flow cytometry. (*a*) For surface H-2K^b expression, R8, L-K^b-high, or L-K^b-low APCs were stained with a H-2K^b-specific mAb. (*b*) For surface H-2K^b/SIINFEKL complex expression, R8, L-K^b-high, or L-K^b-low APCs were cultured overnight in the presence of SIINFEKL-peptide and then stained with a mAb specific for the H-2K^b/SIINFEKL complex. Surface expression data were standardized by assigning a relative expression value of 1 to R8 cells on each measurement. Data are means of three independent experiments ± SD.

Purified Plate-Bound pMHCs Restore Activation of T Cell Hybridomas Expressing TCR Mutants with Prolonged TCR–pMHC Interaction Half-Lives. To maximize pMHC ligand density, soluble H-2K^b/VSV complexes were produced and biotinylated as described (40). These molecules were added on streptavidin-coated ELISA plates and used to evaluate activation of T cell hybridomas (40). By this approach, known amounts of cognate pMHCs can be used to challenge T cell hybridomas in the absence of pMHCs containing other peptides, such as endogenous peptides present on APCs. Thus, plate-bound pMHC molecules might represent a more accurate approach to correlate antigen density with T cell activation, as compared with exogenously added peptide to APCs. As shown in Fig. 4*a*, plate-bound H-2K^b/VSV complexes were able to activate the WT N30.7 T cell hybridoma, as well as TCR mutant G97A. The amount of IL-2 secreted by these cell lines is comparable to that secreted in response to VSV-pulsed APCs (Fig. 2 *a* and *b*). Consistent with our previous results, TCR mutant G97A showed higher IL-2 release compared with the WT TCR (Fig. 4*a*). However, a significant phenotypic change was observed for TCR mutants G97/99A and G99A, which have extended TCR–pMHC interaction $t_{1/2}$ with H-2K^b/VSV (Table 3). T cell hybridomas expressing each of these mutant TCRs were efficiently activated and released significant amounts of IL-2 upon stimulation with H-2K^b/VSV bound to plastic plates (Fig. 4 *b* and *c*). This reversion in function was limited only to TCR mutants with TCR–pMHC

IMMUNOLOGY

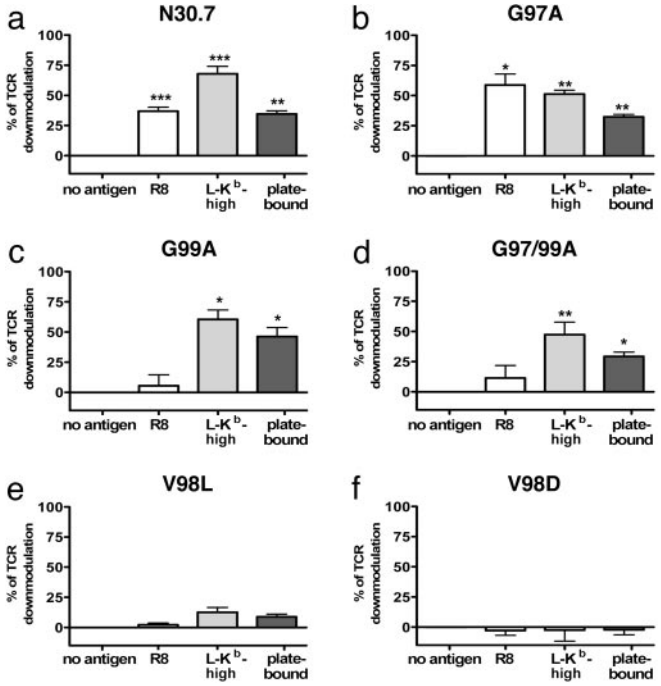

Fig. 5. TCR down-modulation is also modulated by the TCR–pMHC interaction half-life and cognate pMHC density. Surface TCR down-modulation was measured for T cell hybridomas expressing the WT or one of the CDR3β mutant TCRs in response to VSV peptide–pulsed R8 cells, L-K^b-high cells, or plate-bound H-2K^b/VSV complexes. T cell hybridomas were cocultured with an equal number of VSV peptide-pulsed APCs or 1 μg of plate-bound H-2K^b/VSV complexes. After 5 h, FACS analysis was performed on harvested cells staining for CD8α and TCR-β. Data are means of three independent experiments ± SD (*, $P < 0.05$; **, $P \leq 0.01$; ***, $P < 0.001$).

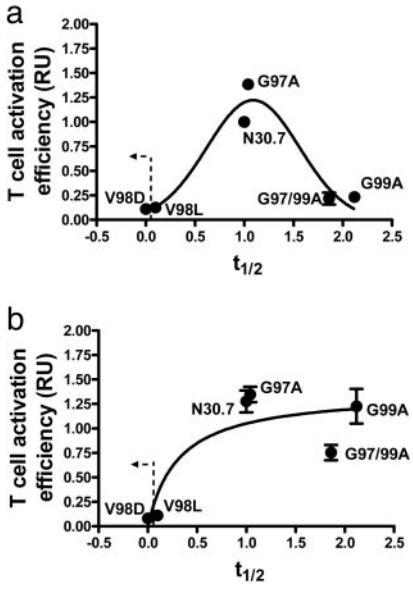

Fig. 6. T cell activation as a function of TCR–pMHC dwell time is modulated by cognate pMHC density on the APC surface. (*a*) A Gaussian distribution is obtained for T cell activation and $t_{1/2}$ data points at low pMHC density on the APC surface. (*b*) A hyperbolic distribution is obtained for T cell activation and $t_{1/2}$ data points at high pMHC density on the APC surface. Plotted T cell activation data points were obtained from IL-2 release results in response either to R8 or L-K^b-high APCs pulsed with 10 μM VSV-peptide. An arbitrary value of 1 was assigned to the IL-2 release of N30.7 hybridoma in response to R8 cells pulsed with 10 μM VSV-peptide.

interaction $t_{1/2}$ longer than the WT N30.7 TCR. Accordingly, neither T cell hybridomas expressing mutant TCR V98L that binds to the ligand with a shorter $t_{1/2}$ nor TCR mutant V98D that does not bind H-2K^b/VSV released IL-2 in response to plastic-bound H-2K^b/VSV complexes (Fig. 4 *d* and *e*).

TCR Internalization Is also Modulated by TCR–pMHC Interaction Half-Lives and Cognate pMHC Density. To measure an early event involved in T cell activation, we evaluated TCR down-modulation in response to VSV peptide-loaded APCs. This process is characteristic of productive TCR engagement by agonist ligands (20, 41). In a 5-h assay with R8 cells as APCs, TCR down-modulation was observed only for the WT N30.7 TCR and TCR mutant G97A (Fig. 5 *a* and *b*). T cell hybridomas expressing TCR mutants G97/99A, G99A, V98L, and V98D did not significantly internalize their TCRs upon incubation with VSV peptide-loaded R8 cells (Fig. 5 *c–f*). This result was consistent with the finding that these TCR mutants were impaired for IL-2 release in response to VSV peptide-pulsed R8 cells (Fig. 2 *c–f*).

In agreement with their higher H-2K^b expression, VSV-pulsed L-K^b-high cells were more efficient at inducing internalization of WT N30.7 TCR than were VSV-pulsed R8 cells (Fig. 5*a*). As expected, TCR mutant G97A was also efficiently internalized in response to VSV-pulsed L-K^b-high cells, although no significant difference was observed when compared with R8 cells (Fig. 5*b*). Consistent with their IL-2 secretion pattern in response to VSV-pulsed L-K^b-high cells (Fig. 2 *c* and *d*), TCR mutants G97/99A and G99A, both with prolonged $t_{1/2}$, significantly internalized their surface TCRs when stimulated with VSV-pulsed L-K^b-high cells (Fig. 5 *c* and *d*). On the other hand, TCR mutant V98L, which has a short $t_{1/2}$ of interaction with H-2K^b/VSV, and V98D, which does not bind H-2K^b/VSV, showed no significant TCR internalization (Fig. 5 *e* and *f*) in response to VSV-pulsed L-K^b-high cells. These results are in agreement with the IL-2 secretion patterns shown by TCR mutants V98L and V98D in response to VSV-pulsed R8 or L-K^b-high cells (Fig. 2 *e* and *f*).

Finally, we evaluated surface TCR internalization for T cell hybridomas stimulated with purified H-2K^b/VSV complexes bound to plastic plates. In this case, as observed with VSV-pulsed L-K^b-high cells, significant TCR internalization was observed for the WT N30.7 TCR, as well as for TCR mutants G97A, G97/99A, and G99A (Fig. 5 *a–d*). These results are consistent with the IL-2 secretion pattern observed for these TCRs in response to plate-bound H-2K^b/VSV complexes (Fig. 4 *a–c*). As expected no significant TCR internalization was observed for TCR mutants V98D and V98L (Fig. 5 *e* and *f*), which did not secrete IL-2 in response to plastic-bound H-2K^b/VSV (Fig. 4 *d* and *e*).

An Optimal Dwell Time Is Not Required for T Cell Activation at High Cognate pMHC Density. When T cell activation data for each TCR mutant are plotted against their relative interaction $t_{1/2}$ with H-2K^b/VSV, different curve shapes are obtained depending on whether T cells are stimulated with low or high epitope density on the APC surface (Fig. 6). As previously reported by us, T cell activation displays a Gaussian distribution as a function of the TCR–pMHC interaction $t_{1/2}$ at low-medium epitope density (R8 cells as APCs, Fig. 6*a*) (19). However, when T cell activation assays were performed with high epitope densities (VSV-pulsed L-K^b-high cells as APCs or pMHC-coated plates) a hyperbolic curve was observed (Fig. 6*b*).

Discussion

Previous data from our group showed a peak in the plot of TCR–pMHC interaction $t_{1/2}$ versus T cell activation, measured either by TCR internalization or IL-2 release. These observations are consistent with the notion that efficient T cell activation by

pMHC occurs only within a range of $t_{1/2}$ for the TCR–pMHC interaction. According to this model, TCRs that bind to pMHC with excessively short $t_{1/2}$ would fail to complete the intracellular signaling cascade, whereas TCRs that bind to pMHC with excessively long $t_{1/2}$ would interfere with TCR serial engagement (19, 20). This was the case for stimulation of T cells with a specific cognate pMHC density available on the surface of R8 cells, which are heterozygous for the H-2 locus. Here, we generalized our observations by systematically varying the density of expression of H-2K^b, using either L cells stably transfected with H-2K^b as APCs or plate-bound purified H-2K^b molecules. As proposed by our mathematical model and supported by our experimental data for IL-2 secretion and TCR internalization, high epitope densities can efficiently restore T cell activation only for those T cell hybridomas expressing mutant TCRs with prolonged TCR–pMHC interaction $t_{1/2}$. Although at high cognate pMHC densities T cell hybridomas expressing TCRs with short $t_{1/2}$ of interaction with pMHC remained unresponsive, those expressing TCRs with prolonged $t_{1/2}$ of interaction were efficiently activated. One explanation for the observed restoration of activation for those hybridomas expressing TCR mutants with prolonged $t_{1/2}$ by high epitope density could be a reduced requirement for TCR serial engagement (6, 13). Whereas T cell activation by low pMHC density would require several TCR molecules to be serially engaged by one single pMHC molecule and would be impaired by an excessively long TCR–pMHC dwell time, no such requirement would hold when cognate pMHC is abundant on the APC surface. It is likely that at high epitope density the intracellular signaling threshold needed for T cell activation could be achieved by simultaneous engagement of multiple TCRs by abundant cognate pMHC on the APC surface. In our experimental conditions, this simultaneous TCR engagement leads to activation only of those T cells expressing TCRs with intermediate and prolonged $t_{1/2}$ (T cell hybridomas N30.7, G97A, G97/99A, and G99A). No restoration of activation of T cell hybridomas expressing TCR mutants with short $t_{1/2}$ of TCR–pMHC interaction was observed. These data are consistent with results from a previous study showing a linear correlation between TCR affinity and T cell activation when purified TCR ligand was bound to plastic plates (42). Inhibition of T cell activation by increased $t_{1/2}$ of TCR–pMHC interaction has been demonstrated on several TCR systems, indicating that it seems to be a broad phenomenon (19, 27, 29, 32, 43). The fact that no significant TCR affinity maturation occurs during T cell responses to pathogens (31) and the observation that T cell clones with high-affinity TCRs show impaired function (32, 33) underscore the important effect on the immune response that inhibition by long TCR–pMHC dwell time has. However, different models have been proposed based on data obtained from experiments performed with pMHC or TCR mutants derived from either the 2B4 or 2C TCR systems (44, 45). Although most TCR or peptide mutations that extended the $t_{1/2}$ for the 2C TCR-pMHC or 2B4 TCR–pMHC interaction led to an increase in T cell reactivity, some of them caused reduced T cell activation as compared with TCRs with shorter $t_{1/2}$ (44, 45). Considering that these studies included peptide variants that bind with different stability to MHC it seems possible that differential pMHC densities could influence these results. Our data suggest that under experimental conditions consisting of high-density pMHC, either on the APC surface or bound to plastic plates, it would be expected that TCR–pMHC interactions with long half-lives lead to efficient T cell activation.

Taken together, our mathematical simulation model and experimental data support the notion that at low epitope density, which is considered as most physiologically relevant, an optimal TCR–pMHC dwell time would be required for productive T cell activation. Thus, both kinetic proofreading and serial engagement would be required for T cell activation. On the other hand, at high cognate pMHC density, simultaneous engagement of several TCR molecules could occur, thus overriding the requirement for serial engagement.

We thank Drs. M. Roden, D. Brims, and E. Lazar for help with the manuscript and R. N. Germain for providing the 25-D1.16 hybridoma. This work was supported by Fondo Nacional de Investigación Científica y Tecnológica Grants 1030557 and 7030038 (to A.M.K.), Dirección General de Postgrado, Investigación, Centros y Programas Grant 2002/11E (to A.M.K.), International Foundation for Science Grant A/3639-1 (to A.M.K.), Fondo de Investigación Avanzada en Areas Prioritarias Grant 13980001 (to A.M.K.), National Institutes of Health Grants AI07289, R01DK65247, and T32CA09173 (to S.G.N.) and R37-GM35556 (to B.G.), and the U.S. Department of Energy through Contract W-7405-ENG-36 (to B.G.).

1. Kalergis, A. M. (2003) *Curr. Pharm. Des.* **9,** 233–244.
2. Garcia, K. C., Teyton, L. & Wilson, I. A. (1999) *Annu. Rev. Immunol.* **17,** 369–397.
3. Kalergis, A. M. & Nathenson, S. G. (2000) *J. Immunol.* **165,** 280–285.
4. Eisen, H. N., Sykulev, Y. & Tsomides, T. J. (1996) *Adv. Protein Chem.* **49,** 1–56.
5. Sykulev, Y., Joo, M., Vturina, I., Tsomides, T. J. & Eisen, H. N. (1996) *Immunity* **4,** 565–571.
6. Valitutti, S. & Lanzavecchia, A. (1997) *Immunol. Today* **18,** 299–304.
7. Gewurz, B. E., Gaudet, R., Tortorella, D., Wang, E. W., Ploegh, H. L. & Wiley, D. C. (2001) *Proc. Natl. Acad. Sci. USA* **98,** 6794–6799.
8. Tobar, J. A., González, P. A. & Kalergis, A. M. (2004) *J. Immunol.* **173,** 4058–4065.
9. Johnson, W. E. & Desrosiers, R. C. (2002) *Annu. Rev. Med.* **53,** 499–518.
10. Lorenzo, M. E., Ploegh, H. L. & Tirabassi, R. S. (2001) *Semin. Immunol.* **13,** 1–9.
11. Restifo, N. P., Esquivel, F., Kawakami, Y., Yewdell, J. W., Mule, J. J., Rosenberg, S. A. & Bennink, J. R. (1993) *J. Exp. Med.* **177,** 265–272.
12. Kageshita, T., Hirai, S., Ono, T., Hicklin, D. J. & Ferrone, S. (1999) *Am. J. Pathol.* **154,** 745–754.
13. Valitutti, S., Muller, S., Cella, M., Padovan, E. & Lanzavecchia, A. (1995) *Nature* **375,** 148–151.
14. Valitutti, S., Dessing, M., Aktories, K., Gallati, H. & Lanzavecchia, A. (1995) *J. Exp. Med.* **181,** 577–584.
15. Lanzavecchia, A. & Sallusto, F. (2001) *Nat. Immunol.* **2,** 487–492.
16. Rachmilewitz, J. & Lanzavecchia, A. (2002) *Trends Immunol.* **23,** 592–595.
17. Davis, M. M., Boniface, J. J., Reich, Z., Lyons, D., Hampl, J., Arden, B. & Chien, Y. (1998) *Annu. Rev. Immunol.* **16,** 523–544.
18. van der Merwe, P. A. (2001) *Immunity* **14,** 665–668.
19. Kalergis, A. M., Boucheron, N., Doucey, M. A., Palmieri, E., Goyarts, E. C., Vegh, Z., Luescher, I. F. & Nathenson, S. G. (2001) *Nat. Immunol.* **2,** 229–234.
20. Coombs, D., Kalergis, A. M, Nathenson, S. G., Wofsy, C. & Goldstein, B. (2002) *Nat. Immunol.* **3,** 926–931.
21. McKeithan, T. W. (1995) *Proc. Natl. Acad. Sci. USA* **92,** 5042–5046.
22. Rabinowitz, J. D., Beeson, C., Lyons, D. S., Davis, M. M. & McConnell, H. M. (1996) *Proc. Natl. Acad. Sci. USA* **93,** 1401–1405.
23. Savage, P. A., Boniface, J. J. & Davis, M. M. (1999) *Immunity* **10,** 485–492.
24. Grakoui, A., Bromley, S. K., Sumen, C., Davis, M. M., Shaw, A. S., Allen, P. M. & Dustin, M. L. (1999) *Science* **285,** 221–227.
25. Kersh, G. J., Kersh, E. N., Fremont, D. H. & Allen, P. M. (1998) *Immunity.* **9,** 817–826.
26. Lanzavecchia, A., Lezzi, G. & Viola, A. (1999) *Cell* **96,** 1–4.
27. Sykulev, Y., Vugmeyster, Y., Brunmark, A., Ploegh, H. L. & Eisen, H. N. (1998) *Immunity* **9,** 475–483.
28. Hudrisier, D., Kessler, B., Valitutti, S., Horvath, C., Cerottini, J. C. & Luescher, I. F. (1998) *J. Immunol.* **161,** 553–562.
29. Kessler, B. M., Bassanini, P., Cerottini, J. C. & Luescher, I. F. (1997) *J. Exp. Med.* **185,** 629–640.
30. Zal, T., Zal, M. A. & Gascoigne, N. R. (2002) *Immunity* **16,** 521–534.
31. Slifka, M. K. & Whitton, J. L. (2001) *Nat. Immunol.* **2,** 711–717.
32. Ueno, T., Tomiyama, H., Fujiwara, M., Oka, S. & Takiguchi, M. (2004) *J. Immunol.* **173,** 5451–5457.
33. Rubio-Godoy, V., Dutoit, V., Rimoldi, D., Lienard, D., Lejeune, F., Speiser, D., Guillaume, P., Cerottini, J. C., Romero, P. & Valmori, D. (2001) *Proc. Natl. Acad. Sci. USA* **98,** 10302–10307.
34. Itoh, Y., Hemmer, B., Martin, R. & Germain, R. N. (1999) *J. Immunol.* **162,** 2073–2080.
35. Liu, H., Rhodes, M., Wiest, D. L. & Vignali, D. A. (2000) *Immunity* **13,** 665–675.
36. Menne, C., Moller Sorensen, T., Siersma, V., von Essen, M., Odum, N. & Geisler, C. (2002) *Eur. J. Immunol.* **32,** 616–626.
37. von Essen, M., Bonefeld, C. M., Siersma, V., Rasmussen, A. B., Lauritsen, J. P., Nielsen, B. L. & Geisler, C. (2004) *J. Immunol.* **173,** 384–393.
38. Goyarts, E. C., Vegh, Z., Kalergis, A. M., Horig, H., Papadopoulos, N. J., Young, A. C., Thomson, C. T., Chang, H. C., Joyce, S. & Nathenson, S. G. (1998) *Mol. Immunol.* **35,**593–607.
39. Nakagawa, M., Zeff, R. A., Geier, S. S., Bluestone, J. A. & Nathenson, S. G. (1986) *Immunogenetics* **24,** 381–385.
40. Kalergis, A. M., Goyarts, E. C., Palmieri, E., Honda, S., Zhang, W. & Nathenson, S. G. (2000) *J. Immunol. Methods* **234,**61–70.
41. Valitutti, S., Muller, S., Salio, M. & Lanzavecchia, A. (1997) *J. Exp. Med.* **185,** 1859–1864.
42. Andersen, P. S., Geisler, C., Buus, S., Mariuzza, R. A. & Karjalainen, K. (2001) *J. Biol. Chem.* **276,** 33452–33457.
43. Kessler, B., Hudrisier, D., Cerottini, J. C. & Luescher, I. F. (1997) *J. Exp. Med.* **186,** 2033–2038.
44. Holler, P. D. & Kranz, D. M. (2003) *Immunity* **18,** 255–264.
45. Krogsgaard, M., Prado, N., Adams, E. J., He, X. L., Chow, D. C., Wilson, D. B., Garcia, K. C. & Davis, M. M. (2003) *Mol. Cell* **12,** 1367–1378.